PCCP

ROYAL SOCIETY OF CHEMISTRY

PAPER

View Article Online
View Journal | View Issue

Cite this: *Phys. Chem. Chem. Phys.*, 2025, **27**, 19546

Molecular interplay at the PMMA dielectric and C_{13}-BTBT semiconductor interface

Kirill Gubanov, †[a] Dustin Vivod, †[b] Christiane Sauer,[a] Maria Brzhezinskaya,[c] Dirk Zahn[b] and Rainer H. Fink *[ad]

Received 10th July 2025,
Accepted 26th August 2025

DOI: 10.1039/d5cp02629f

rsc.li/pccp

A growing interest towards all-organic electronics emphasized the importance of interfaces between the functional components of such devices. In particular, the interaction between the dielectric and semiconductor plays a critical role in device functionality, with strong dependency of charge carrier accumulation and mobility on semiconductor molecular arrangement. We report on the beneficial adsorption conformation with a nearly upright standing molecular orientation of a 2-tridecyl-[1]benzothieno[3,2-*b*][1]benzothiophene (C_{13}-BTBT) semiconductor monolayer deposited on Langmuir–Blodgett-prepared polymethyl methacrylate (PMMA) dielectric films. Such an alignment favors a smooth transfer of charge carriers due to the optimal orbital overlap between π-conjugated BTBT units. Atomistic insights into the C_{13}-BTBT/PMMA system through molecular dynamics revealed an advantageous direct contact of the charge-transporting BTBT unit with PMMA, while the alkyl chain is pointing outwards. Compared to non-alkylated BTBT, we demonstrate a 43% lower stiffness for surface-exposed alkyl chains of a C_{13}-BTBT monolayer, as determined by force-distance analysis, highlighting the advantage for flexible device applications. These insights open new perspectives for further engineering of advanced interfaces, paving the way for innovations in efficient carbon-based electronics.

Introduction

The field of organic electronics attracts lots of attention due to the benefits stemming from inexpensive and accessible solution-processability, minimal environmental impact and versatile chemical tunability.[1–3] In this regard, all-carbon-based organic circuitry is of great interest.[4,5] The interfaces between main functional layers play a fundamental role in performance and efficiency of such devices.[6] In particular, a junction between the dielectric and organic semiconductor exists in various electronic systems, such as solar cells, organic light-emitting diodes (OLEDs) or organic field-effect transistors (OFETs).[7–9] This interfacial region significantly influences charge transport, and thus becomes a central factor in optimizing the device functionality and enhancing overall performance.[10]

In the process of interface engineering, the material selection remains a critical aspect.[11] The surface characteristics of the dielectric, such as polarity and chemical composition, impact the formation of an interfacial dipole, further affecting the electronic properties and charge transport in the active channel.[12] In that sense, the use of organic-based dielectrics, such as polymethyl methacrylate (PMMA) can offer an energetically more compatible interface with organic semiconductors, in contrast to the inorganic counterparts.[13–15] Recently, we demonstrated that Langmuir–Blodgett (LB) solution-processability of PMMA offers production of ultrathin high-quality dielectric layers, with its successful incorporation into OFET circuitry.[16] Combined with sufficient electrical resistivity and suitable relative permittivity comparable to established insulators (*e.g.*, SiO_2), PMMA emerges as a suitable candidate as a dielectric in the engineering of all-organic interfaces.[17–19]

At the same time, the surface of the insulator plays an important role in molecular organization of the semiconducting organic layer that forms on top, thereby shaping the overall device functionality.[20] A proper molecular arrangement of the semiconductor facilitates efficient charge transport, and reduces the number of surface sites, thus leading to enhanced switching characteristics.[21] With the great number of reported organic semiconductors, a particular interest was garnered by the emergence of thiophene-based conjugated π-systems of [1]benzothieno[3,2-*b*][1]-benzothiophene (BTBT), which exhibits

[a] *Department of Chemistry and Pharmacy, Friedrich-Alexander-Universität Erlangen-Nürnberg, Egerlandstraße 3, 91058 Erlangen, Germany. E-mail: rainer.fink@fau.de*
[b] *Computer-Chemie-Centrum and Chair of Theoretical Chemistry, Friedrich-Alexander-Universität Erlangen-Nürnberg, Nägelsbachstraße 25, 91052 Erlangen, Germany*
[c] *Helmholtz-Zentrum Berlin für Materialien und Energie, Albert-Einstein-Straße 15, 12489 Berlin, Germany*
[d] *Interdisciplinary Center for Molecular Materials (ICMM, Friedrich-Alexander-Universität Erlangen-Nürnberg, Egerlandstraße 3, 91058 Erlangen, Germany*
† Authors contributed equally.

high charge carrier mobilities (up to 2.0 $cm^2 V^{-1} s^{-1}$).[22] Later developments suggested several strategies aimed at enhancing the efficiency of BTBT-based semiconductors, including the substitution with various radicals.[23] In particular, the incorporation of long alkyl chains drastically enhanced solubility in common solvents, enabling optimized solution-based deposition and leading to improved film morphology with higher structural order and a reduced number of defects.[24] The charge-carrier mobility in alkylated BTBT derivatives was found to strongly depend on the number of carbon atoms within the chains.[25] Longer alkyl chains lead to the intrinsic disorder reduction, improving transport balance, enabling strong intermolecular charge transfer and weak electron–phonon coupling, all of which make these compounds excellent high-mobility organic semiconductors.[26] In the course of ongoing improvements, Tsutsui *et al.* demonstrated that devices using bi-alkylated BTBT units with long alkyl chains (C_n-BTBT-C_n, with n = 12) show remarkably high charge-carrier interfacial mobilities (170 $cm^2 V^{-1} s^{-1}$).[27] However, extending the alkyl chain beyond 13 carbon atoms disrupts the optimal balance between solubility and charge-carrier mobility, leading to a simultaneous decrease of both properties.[28]

In contrast to symmetrically bi-substituted C_n-BTBT-C_n derivatives, a structural composition of mono-alkylated C_{13}-BTBT molecules may favor different adsorption conformations upon deposition on PMMA surface. This, in turn, can significantly impact the charge-transport. The BTBT unit enables efficient movement of the charge carriers along its core, thereby serving as the primary contributor to the charge-transport properties of the molecule.[29] In contrast, the alkyl chain serves mainly to improve solubility and optimize the film formation during solution-processing.[30] It does not participate in charge transport, as long hydrocarbon chains do not have the necessary electronic structure for charge conduction.[31] If the BTBT core is in contact with PMMA, this allows for better orbital overlap at the interface, enabling more efficient accumulation of charge carriers. Alternatively, if the alkyl chains are in contact with PMMA, they form an insulating spacer layer by increasing the effective distance between the dielectric and BTBT π–π stacks, hindering the efficient charge accumulation.[32]

In this study, we combine a comprehensive spectro-microscopic approach with molecular dynamics (MD) simulations to investigate the interfacial interactions between a mono-alkylated C_{13}-BTBT monolayer and Langmuir–Blodgett (LB)-prepared PMMA films. Recent work by Hawly *et al.* demonstrated that mono-substituted C_{13}-BTBT preferentially results in a bilayer-type packing motif, when processed *via* solution-based self-assembly at the liquid–liquid interface.[33] Such a configuration prevents direct probing of the semiconductor–dielectric interface. In order to achieve a monolayer formation, we employed physical vapor deposition (PVD), enabling production of a single C_{13}-BTBT layer. Notably, both MD simulations and force–distance atomic force microscopy (FD AFM) measurements revealed that the BTBT core, rather than the alkyl chain, is in direct contact with the PMMA surface. Further support for the molecular arrangement was obtained through X-ray based angular-dependent spectroscopy from which we derived a clear dichroic effect, indicating a preferential near-upright-standing molecular orientation of the C_{13}-BTBT molecules at the PMMA surface—an advantageous alignment particularly relevant for the unconventional application of polymer dielectric surfaces. Compared to its non-alkylated counterpart, the C_{13}-BTBT monolayer exhibits an enhanced conformational flexibility of the surface-exposed long alkyl side chains.[34] This elasticity character makes the alkylated derivative especially well-suited for use in flexible electronic applications. Overall, our findings provide a foundation for the rational design of optimized organic–dielectric interfaces, contributing to the advancement of high-performance, mechanically compliant organic electronic systems.

Experimental

Interface fabrication

PMMA (purchased from Sigma-Aldrich, as analytical standard) dielectric layers were produced *via* Langmuir–Blodgett (LB) fabrication. 30 μl solution of 10 mg PMMA (20.000M_w) in 1 ml of toluene were evenly distributed over the water subphase at different areas. The compression was initiated with a speed of 20 mm min^{-1} and 60 mN m^{-1} target pressure. A silicon wafer with 5 μm Ti adhesive layer and 100 nm gold on top was used as a substrate. The wafer was lifted by the dip coater (Kibron Layer X) at a speed of 4 mm s^{-1}, only after the pressure–area isotherm indicated 10 compressions (corresponding to approximately 12 nm). Film collection was further carried out without interrupting the barrier motion. The active (sub)monolayers of C_{13}-BTBT and BTBT semiconductors were both fabricated *in situ via* physical vapor deposition (PVD) in the preparation vacuum chamber of HE-SGM beamline. Sublimation of C_{13}-BTBT was carried out at pressure of 10^{-8} mbar with a deposition rate of 0.15 Å s^{-1}. The material deposition was monitored through a quartz crystal microbalance (QCM) until a nominal thickness of (sub)monolayer in each case was reached to avoid bilayer formation.

Characterization tools

Force–distance atomic force microscopy (FD AFM) was carried out using a JPK NanoWizard 4 system in contact mode, utilizing Tap150-G silicon probes of triangular pyramid tip shape with 10 nm radius (purchased from NanoAndMore GmbH, Wetzlar, Germany), no additional coating, resonance frequency of 150 kHz and force constant of 5 N m^{-1}. The JPK data processing tool was used for the analysis of height profiles, FD curves and the application of filters for all measured AFM micrographs. Near-edge X-ray absorption fine structure (NEXAFS) and X-ray photoelectron (XPS) spectra were recorded in partial-electron yield mode at the HE-SGM beamline at the BESSY II storage ring at the Helmholtz-Zentrum for Materials and Energy (HZB Berlin, Germany).[35] All recorded spectra were plotted using Origin 2022, (Version 9.9.0.225). CasaXPS processing software was used for XPS spectra analysis. A detailed

description of the force-field molecular dynamics (MD) simulations procedure can be found in SI Section.

Results and discussion

Force–distance AFM micro-spectroscopic analysis of C_{13}-BTBT adsorption confirmation

Considering the structural composition of the mono-alkylated C_{13}-BTBT semiconductor, we aimed to determine which part of the molecule interfaces with the PMMA surface upon deposition. This distinction—whether the charge-transporting BTBT core or the alkyl side chain is in direct contact with the dielectric—has implications for device performance, as it may affect interfacial dielectric polarization and charge accumulation. Fig. 1a shows a schematic illustration of the two considered interaction configurations between the C_{13}-BTBT monolayer and PMMA films. Note, that we ruled out the possibility of the semiconductor molecule adopting a parallel orientation relative to the dielectric surface. Such configuration is favored on metal substrates due to a strong π-interaction of the aromatic BTBT core with metal electrons. To directly probe the interface, we deposited an organic monolayer onto the LB-prepared PMMA film *via* PVD thus having control over the deposited film thickness. To investigate the molecular arrangement of the semiconductor, we employed FD AFM, where both mono- and non-substituted BTBT molecules were used for direct comparison.

Recent advances in FD-spectroscopy enabled us to combine high-resolution imaging with quantitative analysis of physical interactions. Fig. 1b compares the FD curves obtained for both semiconductors on PMMA surface. Approximately twofold higher degree of adhesion signal observed for BTBT compared to C_{13}-BTBT presumably arises from the differences in nature of the molecular groups directly probed by the AFM tip: in the case of BTBT, the tip interacts with the conjugated core, while for C_{13}-BTBT, it probes the alkyl chain. Given the significant difference between the derived curves, we conclude that in case of the mono-alkylated BTBT deposition, the alkyl chain is oriented away from the surface, while the BTBT core is in direct contact with PMMA. Note, that we excluded variations within the PMMA surface composition as a source of differences in the measured adhesions, since the dielectric surface was characterized prior to the deposition of BTBT and C_{13}-BTBT, demonstrating a consistent average degree of adhesion of approximately 9–10 nN (Fig. S1).

AFM micrographs served as both morphology maps and as spatial guides for extracting FD curve datasets (10 per sample, indicated by green markers), capturing the measurements from various surface regions. Fig. 1c shows the AFM micrograph of a C_{13}-BTBT (sub)monolayer deposited on LB-prepared PMMA. The semiconductor film exhibits a height of approximately 3–3.5 nm, consistent with reported monolayer values.[36] The surface of mono-alkylated BTBT displays a slightly higher average roughness (based on 10 cross-sectional profiles) than the underlying dielectric, with a difference of ∼0.5 nm. A complete BTBT monolayer (Fig. 1d) shows similar average roughness to that of C_{13}-BTBT, yet features a distinct morphology, which may be attributed to the differences in the molecular organization of the top layer part.

In addition, the Young's modulus was derived by fitting the approach-segment of the FD curve, where the tip is compressing the sample (marked with yellow dashed line in Fig. 1b) according to the Hertz–Sneddon model. The surface stiffness of the C_{13}-BTBT monolayer (52.9 MPa) is noticeably lower than that of the non-alkylated BTBT monolayer (92.8 MPa), representing a ∼43% difference in elasticity, due to the flexible nature of the surface-exposed alkyl chains. Given the nanoscale thickness of these films, such difference is mechanically significant and can play a crucial role in enhancing flexibility for device applications.

X-ray-based photon energy- and angle-dependent spectroscopic insight into C_{13}-BTBT molecular orientation

After confirming the favorable adsorption conformation of C_{13}-BTBT, we aimed to determine whether the semiconductor

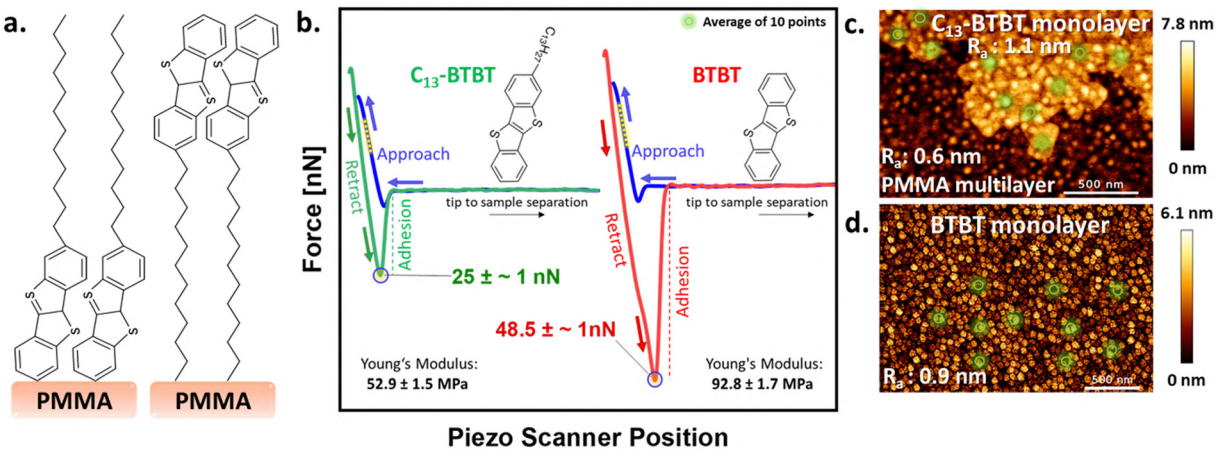

Fig. 1 (a) Scheme of proposed possible C_{13}-BTBT interaction with PMMA surface. (b) FD AFM comparison of the C_{13}-BTBT and non-alkylated BTBT monolayers deposited *via* PVD on LB-PMMA films with respective (c) and (d) AFM micrographs, serving as maps for FD curves extraction.

molecules adopt a preferential orientation on the PMMA surface. Fig. 2a shows angular-dependent near-edge X-ray absorption fine-structure (NEXAFS) spectroscopy measurements, recorded at the carbon K-edge for both PMMA and C_{13}-BTBT. The reference C K-NEXAFS spectra of PMMA (orange curve) shows four main resonances, consistent with previously reported studies.[37] The small resonance at 285.4 eV is associated with C 1s → π* (C═C) transitions, arising from C═C bonds, formed in damaged parts of the polymer backbone, due to PMMA radiation damage. The resonance at 288.1 eV belongs to C 1s → σ* (C–H) transitions. The characteristic fingerprint for PMMA is assigned to the sharp transition near 288.8 eV to the prominent C 1s → π* (C═O) resonance. Spectral features after 292.6 eV arising from various C 1s → σ* (C–C) transitions, with 302.9 eV corresponding to C 1s → σ* (C═O) excitations.

Carbon K-edge NEXAFS spectra of C_{13}-BTBT have been thoroughly investigated in previous studies, with all major resonances and their corresponding electronic transitions reliably assigned.[33] The spectra obtained in this work are consistent with these earlier reports, confirming the characteristic spectroscopic features of the molecule. The C K-NEXAFS spectrum of C_{13}-BTBT deposited on PMMA exhibits three symmerty-equivalent π*-resonances centered around 285.5 eV, which is attributed to C 1s → π*-orbital transitions associated with the conjugated BTBT core.[33] Transitions near the ionization threshold, around 289 eV, are of hybrid character, typically encompassing both C 1s → σ* (C–H) transitions from the terminal alkyl chain and C 1s → π* (C═C) transitions. Post-edge features observed around 294 eV are predominantly attributed to C 1s → σ* (C–C) transitions originating from the C_{13}-chain. Given that NEXAFS absorption is maximized at the lowest angle—where the electric field vector aligns parallel to the C–C bond axis—the data indicate that the alkyl chains are oriented predominantly perpendicular to the substrate surface.

In addition, polar angle-dependent C K-NEXAFS spectra of C_{13}-BTBT monolayer demonstrates a clear linear dichroism, enabling the estimation of the average orientation of the BTBT core relative to the surface normal (Fig. 2b). By fitting the intensity of the sharp π resonance at 285.5 eV (marked with an arrow in Fig. 2a)—attributed to excitations within the conjugated BTBT core—an average tilt angle $\varphi = 15 \pm 2^\circ$ with respect to the surface normal was derived for the BTBT subunit. This result confirms a close-to-upright molecular orientation of the C_{13}-BTBT monolayer on the PMMA – an advantageous arrangement particularly relevant for the unconventional polymer dielectric surfaces. Such conformation is considered favorable for the charge transport, as it promotes efficient intralayer π–π orbital overlap between neighboring BTBT units.[38]

To further investigate the interfacial conformation between C_{13}-BTBT and PMMA, angular-dependent XPS was performed. Fig. 2c shows a clear trend in the intensity of the S 2p peak, measured at normal and grazing emission at 650 eV photon energy. The intensity for normal emission is significantly higher compared to grazing emission as S 2p electrons emitted from the buried BTBT subunit are damped on their longer pathway through the alkane layer. Thus, angular-dependent measurements confirm that BTBT are closer to the PMMAas depicted in the molecular sketch in Fig. 2c.

Molecular dynamics simulations

In order to get some atomistic insights into the interplay of C_{13}-BTBT and PMMA at the interface, molecular dynamics (MD) simulations were carried out. By running two types of setups, one with the BTBT unit in contact with the PMMA (Fig. 3a and b) and one with the alkyl chain (Fig. 3c and d), we performed (2 × 4) series of independent relaxation runs and identified the favored configuration on the basis of energy averages. Each MD simulation was started from placing a 20 × 20 array of C_{13}-BTBT on the PMMA substrate. Upon relaxation, we find the molecules at the edges of the deposited monolayer patch to deform quite significantly. In order to characterize the bulk behavior as representative for a larger film, the adsorption energy was therefore sampled only for a 'core' domain of an 8 × 8 array in the center of the C_{13}-BTBT monolayer patch (Fig. 3a–d colored highlights). Detailed information of the simulation setups, the molecular mechanics models and the applied analyses methods can be found in the supplementary section.

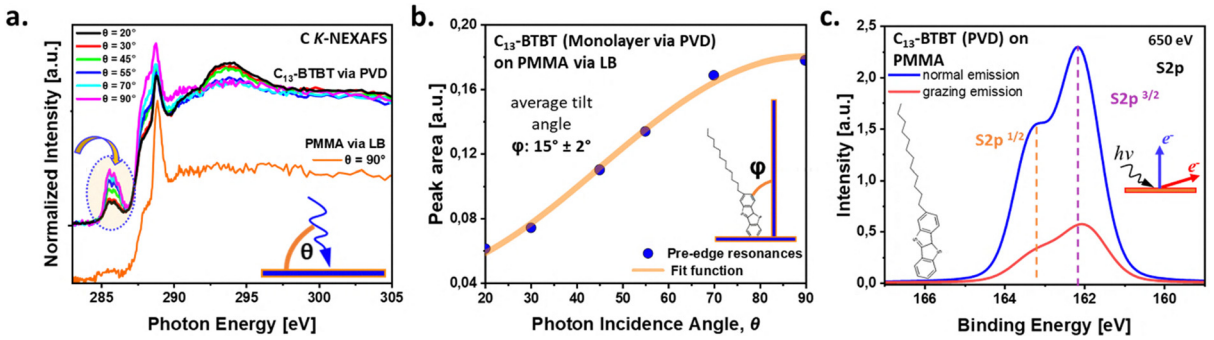

Fig. 2 X-ray-based spectroscopic characterization of C_{13}-BTBT monolayer in direct comparison with BTBT core. (a) Polar angle-dependent C K-NEXAFS spectra of the PVD produced C_{13}-BTBT monolayer on PMMA surface with (b) tilt angle derivation of the C_{13}-BTBT molecular orientation from C 1s → π* resonance intensities. (c) Angle-dependent S 2p XPS spectra of the PVD prepared C_{13}-BTBT (sub)monolayer on PMMA.

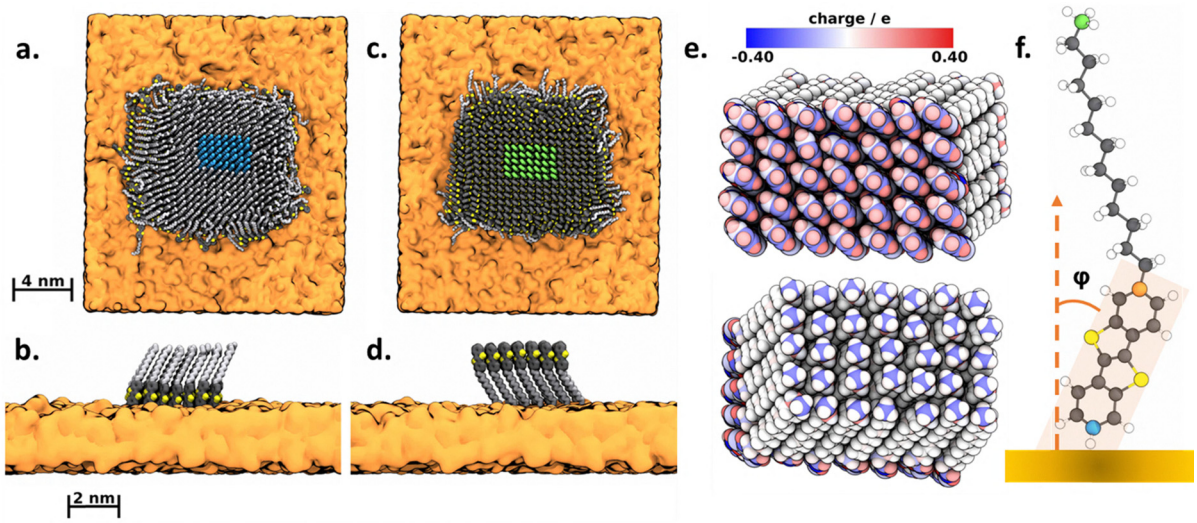

Fig. 3 Exemplary snapshots of the two BTBT setups. (a) A top-down view of the BTBT units in contact with a (b) sideview of only the core molecules. (c) A top-down view of the alkyl chain in contact with a (d) sideview of only the core molecules. PMMA substrate shown in orange, alkyl chains shown in silver, carbon atoms of the BTBT groups shown in black, and sulfur atoms shown in yellow. Hydrogen atoms are omitted for clarity. (e) Exemplary snapshot of the BTBT (top) and alkyl (bottom) contacting the PMMA, with atoms colored according to their charge. (f) C_{13}-BTBT with highlighted carbon atoms. The vector between the blue and orange colored carbon atoms defines the vector used for the calculation of the tilt angle of the BTBT subunit. The vector between the orange and green colored carbon atoms defines the vector used for the calculation of the tilt angle of the alkyl chain. Carbon atoms shown in black, sulfur atoms shown in yellow, and hydrogen atoms shown in white.

For each of the 2 × 4 = 8 BTBT–PMMA interface models investigated, the adsorption energy E_{ads} was sampled individually from:

$$E_{ads} = \langle E^{core}_{BTBT-PMMA} - (E_{PMMA} + E^{core}_{BTBT})\rangle \cdot t \qquad (1)$$

where $E^{core}_{BTBT-PMMA}$ is the potential energy of the system containing the PMMA substrate and the BTBT core molecules, and E_{PMMA} and E^{core}_{BTBT} are two separated systems containing only the PMMA substrate and the monolayer patch of BTBT core molecules, respectively. The suffix t indicates time averages taken from 20 ns production runs, all based on carefully equilibrated model systems as described in the supporting information.

Contrasting the average adsorption energies according to eqn (1) for each type of interface (Table 1), we find those with the BTBT units in contact with the PMMA substrate are energetically more favorable by 0.107 ± 0.013 eV molecule^{-1} (with the error margin taken as the standard deviation from the 4 independent sampling runs). It is interesting to split this potential energy difference into its Lennard-Jones (taken as van-der-Waals interactions) and Coulomb components – which showed energy differences between the two setups of 0.090 ± 0.012 eV and 0.017 ± 0.003 eV per molecule, respectively. The difference in adsorption energy thus originates mainly from the van-der-Waals interactions. To gain further insight into the electrostatic interactions at the interface, including spatial resolution of the charge multipoles, the BTBT and alkyl interfaces are depicted in Fig. 3e using a color code according to their atomic charges. In contrast to the alkyl chains, we find the charge profile of the BTBT moieties more pronounced with the outermost hydrogen atoms exhibiting positive charges – which favorably interact with the negative charge of the PMMA substrate.[39] In turn the overall dipole moment of the C_{13}-BTBT layer is negligible and does not account for the preference of BTBT–PMMA contacts.

Table 1 Adsorption energies (per molecule) of the "core" molecules of the BTBT monolayer with its two contact probabilities with the PMMA substrate according to eqn (1)

Energy component [eV molecule^{-1}]	BTBT contact	Alkyl chain contact
Lennard-Jones	−0.103 ± 0.009	−0.013 ± 0.007
Coulombic	−0.017 ± 0.003	−0.000 ± 0.000
Sum	−0.120 ± 0.010	−0.013 ± 0.007

Additionally, we analyzed key structural features of the interface. The average thickness along the interface normal, root mean square fluctuations (RMSF) of the non-hydrogen atoms of the C_{13}-BTBT film, as well as the areas and tilt angles of the alkyl and BTBT subunits, respectively, are summarized in Table 2. In order to calculate the tilt angle of the BTBT and alkyl subunits of the C_{13}-BTBT, three distinct carbon atoms, as shown in Fig. 3f, have been chosen as vector endpoints. For BTBT–PMMA contacts, the BTBT subunits are tilted by φ = 14 ± 7.8° from the surface normal, whereas alkyl-PMMA contacts show alkyl tilting by 31.8 ± 2.5°, respectively. This is in a good agreement with the experimentally determined tilting of BTBT–PMMA contacts – for which NEXAFS spectroscopy indicates nearly upright orientation.

When comparing the thickness and RMSFs of the core units, we observe that both values are larger for the systems with the BTBT units in contact to the PMMA substrate. These values are a result of the molecules occasionally fluctuating in z-direction as they may enter into local cavities of the PMMA substrate.

Table 2 Structural features of the two different C_{13}-BTBT setups. Only core molecules, as described in methods, have been considered. The first two rows show the mean maximum and minimum distances of the films to the PMMA substrate (Fig. S4). Rows two and three list the areas of the subunits. The rows five and six list the mean angles of the subunits of the core molecules. The last row lists the mean RMSF of the core molecules, excluding hydrogen atoms

Feature of core molecules	BTBT contact	Alkyl chain contact
Z-dist low [Å]	−4.50 ± 0.79	−1.13 ± 0.22
Z-dist high [Å]	22.63 ± 0.79	23.25 ± 0.22
Area BTBT [nm^2]	8.87 ± 0.20	8.48 ± 0.03
Area alkyl [nm^2]	8.45 ± 0.07	8.00 ± 0.08
Angle BTBT [°]	φ = 14.0 ± 7.8	φ = 5.3 ± 2.6
Angle alkyl [°]	φ = 33.0 ± 4.4	φ = 31.8 ± 2.5
RMSF [Å]	1.08 ± 0.12	0.67 ± 0.12

This movement is visualized by *z*-density histograms of the C_{13}-BTBT molecules in Fig. S4, where we also observe a higher penetration depth of the C_{13}-BTBT molecules into the surface cavities of the PMMA substrate. We can thus infer that the entropic contributions are greater for these systems as the C_{13}-BTBT molecules are more mobile and access more space, *i.e.* have more configurations.

Conclusions

We unveil a structurally and electronically favorable all-organic semiconductor/dielectric interface composed of high charge-carrier-mobility C_{13}-BTBT monolayer and a Langmuir–Blodgett-prepared PMMA film, offering new insights into molecular-level interface engineering. Our comprehensive experimental and computational analysis reveals a favorable adsorption conformation, in which the π-conjugated BTBT core interfaces directly with the PMMA surface, while the alkyl chain extends outwards. This configuration minimizes interfacial spacing, thereby promoting efficient charge accumulation and enhancing the overall charge-transport. X-ray-based spectroscopic data further confirm a pronounced dichroism indicative of a preferentially upright molecular orientation, with an average tilt angle of ∼15° from the surface normal—an alignment that optimizes π–π orbital coupling and thus facilitates intralayer charge conduction. These experimental findings are fully supported by molecular dynamics simulations. Additionally, comparative nano-mechanical measurements show a 43% increase in surface elasticity for the mono-alkylated BTBT monolayer relative to its non-substituted counterpart, underscoring its suitability for flexible electronics. Collectively, these results highlight rational approaches for tailoring organic interfaces at the molecular level, paving the way for future advancements in high-performance, mechanically compliant organic electronic devices.

Author contributions

KG, CS and RHF performed major part of the experiments, conceptualized and finalized the manuscript. DV and DZ performed and analyzed MD calculations. MB supported NEXAFS and XPS measurements at the beamline station.

Conflicts of interest

The authors declare no competing interests.

Data availability

All data are available in the main Article and SI. Source data can be provided upon request. Supplementary information: The authors provide additional data within the SI. See DOI: https://doi.org/10.1039/d5cp02629f

Source data are provided upon request.

Acknowledgements

KG and RHF are grateful for the financial support by the Federal Ministry of Education and Research (BMBF, contract 05K22WE2), and "Solar Technologies Go Hybrid" – (SolTech) initiative by the State of Bavaria. KG and RHF acknowledge HZB for beamtime allocation, technical assistance, and traveling support.

References

1 I. McCulloch, M. Chabinyc, C. Brabec, C. B. Nielsen and S. E. Watkins, *Nat. Mater.*, 2023, **22**, 1304–1310, DOI: 10.1038/s41563-023-01579-0.
2 M. Berggren, D. Nilsson and N. D. Robinson, *Nat. Mater.*, 2007, **6**, 3–5, DOI: 10.1038/nmat1817.
3 J. W. Ward, Z. A. Lamport and O. D. Jurchescu, *ChemPhysChem*, 2015, **16**, 1118–1132, DOI: 10.1002/cphc.201402757.
4 K. Watanabe, N. Miura, H. Taguchi, T. Komatsu, A. Aratake, T. Makita, M. Tanabe, T. Wakimoto, S. Kumagai, T. Okamoto, S. Watanabe and J. Takeya, *Adv. Mater. Technol.*, 2024, **9**, 2301673, DOI: 10.1002/admt.202301673.
5 R. L. McCreery, *Acc. Chem. Res.*, 2022, **55**, 2766–2779, DOI: 10.1021/acs.accounts.2c00401.
6 N. Koch, *ChemPhysChem*, 2007, **8**, 1438–1455, DOI: 10.1002/cphc.200700177.
7 F. Guo, A. Karl, Q. F. Xue, K. Cheong Tam, K. Forberich and C. J. Brabec, *Light: Sci. Appl.*, 2017, **6**, e17094, DOI: 10.1038/lsa.2017.94.
8 C. Di, Y. Liu, G. Yu and D. Zhu, *Acc. Chem. Res.*, 2009, **42**(10), 1471–1688, DOI: 10.1021/ar9000873.
9 Y. C. Hsiao, H. Zang, I. Ivanov, T. Xu, L. Lu, L. Yu and B. Hu, *J. Appl. Phys.*, 2014, **115**, 154506, DOI: 10.1063/1.4871466.
10 J. Ren, B. Rong, L. Zheng, Y. Hu, Y. Wang, Z. Wang, X. Chen, K. Zhang, L. Li and W. Hu, *Adv. Funct. Mater.*, 2025, **35**, 2412472, DOI: 10.1002/adfm.202412472.
11 Y. Li, H. Xie, E. L. Lim, A. Hagfeldt and D. Bi, *Adv. Energy Mater.*, 2022, **12**, 2102730, DOI: 10.1002/aenm.202102730.
12 M. Fahlman, S. Fabiano, V. Gueskine, D. Simon, M. Berggren and X. Crispin, *Nat. Rev. Mater.*, 2019, **4**, 627–650, DOI: 10.1038/s41578-019-0127-y.
13 H. Ma, M. S. Liu and A. K. Y. Jen, *Polym. Int.*, 2009, **58**, 594–619, DOI: 10.1002/pi.2572.

14 S. Nam, Y. J. Jeong and J. Jang, *Org. Electron.*, 2020, **85**, 105828, DOI: **10.1016/j.orgel.2020.105828**.
15 S. Sang, L. Li, Q. Li, L. Ding, X. Li, Z. Chang, Y. Chen, R. Ullan, J. Ma and J. Ji, *iScience*, 2024, **27**, 109724, DOI: **10.1016/j.isci.2024.109724**.
16 K. Gubanov, C. Sauer, R. C. Nah, F. Streller, K. E. Dehm, R. W. Crisp, Y. Reva, D. M. Guldi and R. H. Fink, *ACS Appl. Eng. Mater.*, 2025, **3**, 1446–1454, DOI: **10.1021/acsaenm.5c00262**.
17 H. Q. Zhang, Y. Jin and Y. Qiu, *IOP Conf. Ser.: Mater. Sci. Eng.*, 2015, **87**, 012032, DOI: **10.1088/1757-899X/87/1/012032**.
18 M. Na and S. W. Rhee, *Org. Electron.*, 2006, **7**, 205–212, DOI: **10.1016/j.orgel.2006.02.003**.
19 P. Pandit, M. Banerjee and A. Gupta, *Colloids Surf., A*, 2014, **454**, 189–195, DOI: **10.1016/j.colsurfa.2014.04.028**.
20 X. Sun, C. Di and Y. Liu, *J. Mater. Chem.*, 2010, **20**, 2599–2611, DOI: **10.1039/B921449F**.
21 W. H. Lee, J. H. Cho and K. Cho, *J. Mater. Chem.*, 2010, **20**, 2549–2561, DOI: **10.1039/B924415H**.
22 K. Takimiya, I. Osaka, T. Mori and M. Nakano, *Acc. Chem. Res.*, 2014, **47**, 1493–1502, DOI: **10.1021/ar400282g**.
23 M. Sugiyama, S. Jancke, T. Uemura, M. Kondo, Y. Inoue, N. Namba, T. Araki, T. Fukushima and T. Sekitani, *Org. Electron.*, 2021, **96**, 106219, DOI: **10.1016/j.orgel.2021.106219**.
24 M. Alkan and I. Yavuz, *Phys. Chem. Chem. Phys.*, 2018, **20**, 15970, DOI: **10.1039/c8cp01640b**.
25 R. Wawrzinek, J. Sobus, M. U. Chaudhry, V. Ahmad, A. Grosjean, J. K. Clegg, E. B. Namdas and S. C. Lo, *ACS Appl. Mater. Interfaces*, 2019, **11**, 3271–3279, DOI: **10.1021/acsami.8b16158**.
26 P. Xie, T. Liu, J. Sun and J. Yang, *Adv. Funct. Mater.*, 2022, **32**, 2200843, DOI: **10.1002/adfm.202200843**.
27 Y. Tsutsui, G. Schweicher, B. Chattopadhyay, T. Sakurai, J. B. Arlin, C. Ruzié, A. Aliev, A. Ciesielski, S. Colella, A. R. Kennedy, V. Lemaur, Y. Olivier, R. Hadji, L. Sanguinet, F. Castet, S. Osella, D. Dudenko, D. Beljonne, J. Cornil, P. Samorì, S. Seki and Y. H. Geerts, *Adv. Mater.*, 2016, **28**, 7106–7114, DOI: **10.1002/adma.201601285**.
28 H. Ebata, T. Izawa, E. Miyazaki, K. Takimiya, M. Ikeda, H. Kuwabara and T. Yui, *J. Am. Chem. Soc.*, 2007, **129**, 15732–15733, DOI: **10.1021/ja074841i**.
29 H. Usta, D. Kim, R. Ozdemir, Y. Zorlu, S. Kim, M. C. R. Delgado, A. Harbuzaru, S. Kim, G. Demirel, J. Hong, Y.-G. Ha, K. Cho, A. Facchetti and M.-G. Kim, *Chem. Mater.*, 2019, **31**, 5254–5526, DOI: **10.1021/acs.chemmater.9b01614**.
30 W. Park, C. Yun, S. Yun, J. J. Lee, S. Bae, D. Ho, C. Kim and S. Seo, *Org. Electron.*, 2022, **105**, 106508, DOI: **10.1016/j.orgel.2022.106508**.
31 A. Y. Amin, A. Khassanov, K. Reuter, T. Meyer-Friedrichsen and M. Halik, *J. Am. Chem. Soc.*, 2012, **134**, 16548–16550, DOI: **10.1021/ja307802q**.
32 Q. Wei, L. Liu, S. Xiong, X. Zhang, W. Deng, X. Zhang and J. Jie, *J. Phys. Chem. Lett.*, 2020, **11**, 359–365, DOI: **10.1021/acs.jpclett.9b03439**.
33 T. Hawly, M. Johnson, B. Zhao, M. Wu, A. Späth, F. Streller, H. N. Jäkel, M. Halik, E. Spiecker, B. Watts, A. Nefedov and R. H. Fink, *ACS Appl. Electron. Mater.*, 2022, **4**, 12, DOI: **10.1021/acsaelm.2c01095**.
34 N. Shioya, M. Yoshida, M. Fujii, T. Shimoaka, R. Miura, S. Maruyama and T. Hasegawa, *J. Phys. Chem. Lett.*, 2022, **13**, 11918–11924, DOI: **10.1021/acs.jpclett.2c03399**.
35 A. Nefedov and C. Wöll, Surface Science Techniques, *Springer Series in Surface Sciences*, Berlin, Heidelberg, 2013, **51**, pp. 277–303, DOI: **10.1007/978-3-642-34243-1_10**.
36 S. P. Prakoso, Y. J. Ke, D. C. Huang, C. L. Wang and Y. T. Tao, *J. Chin. Chem. Soc.*, 2022, **69**, 440–449.
37 A. D. Winter, E. Larios, F. M. Alagmir, C. Jaye, D. Fischer and E. M. Campo, *Langmuir*, 2013, **29**, 15822–15830, DOI: **10.1021/la404312x**.
38 V. Coropceanu, J. Cornil, D. A. D. S. Filho, Y. Olivier, R. Silbey and J. L. Brédas, *Chem. Rev.*, 2007, **107**, 926–952, DOI: **10.1021/cr050140x**.
39 H. Falahati, L. Wong, L. Davarpanah, A. Garg, P. Schmitz and D. P. J. Barz, *Electrophoresis*, 2014, **35**, 870–882, DOI: **10.1002/elps.201300436**.